Cement and Concrete Research 39 (2009) 14–29

Contents lists available at ScienceDirect

Cement and Concrete Research

journal homepage: http://ees.elsevier.com/CEMCON/default.asp

Rheological properties of cement paste: Thixotropic behavior and structural breakdown

Jon Elvar Wallevik *

Innovation Center Iceland, Department of Concrete Research, Keldnaholti, IS-112 Reykjavik, Iceland

ARTICLE INFO

Article history:
Received 18 July 2008
Accepted 7 October 2008

Keywords:
Cement paste
Rheology
Thixotropy
Structural breakdown

ABSTRACT

In this work, a new material model is presented to simulate rheological behavior of cement paste. This material model is among others based on combined concepts by Hattori and Izumi and by Tattersall and Banfill. More precisely, coagulation, dispersion and re-coagulation of the cement particles (giving a true thixotropic behavior) in combination with the breaking of certain chemically formed linkages between the particles (giving a so-called structural breakdown behavior) are assumed to play an important role in generating the overall time-dependent behavior of the cement paste. The model evaluation is done by comparing experimental data with model prediction.

1. Introduction

Cement paste is a suspension of cement particles in water and represents a good example of a concentrated suspension. Concrete, which is essentially a mixture of cement paste and aggregates, has become the most commonly used structural material in modern civilizations. The quality of the concrete structure is of course dependent on the quality of each constituent used in the concrete mix. However, this is not the only controlling factor. The quality is also much dependent on the rheological behavior of the fresh concrete during placement into formwork at jobsite [1]. Hence, the importance to understand such behavior. In particular, a general connection between the rheological behavior of cement paste and the structural changes governing thixotropy and structural breakdown can provide a better understanding of the different results gained at jobsite. For example, breaking up the so-called static yield stress into different components depending on the mechanism that they originate from, can aid to better understand the nature of the observed reduction in formwork pressure for self-compacting concrete (SCC). An extensive work about the relationship between the static yield stress of SCC and formwork pressure has for example been carried out by Billberg [2].

1.1. Thixotropic behavior

The model introduced here is based on thixotropic behavior as well as on a certain process called "structural breakdown" (the latter is explained in Section 1.2). The interest in the former phenomena is nearly as old as modern rheology [3]. An increasing number of real materials have been found to show thixotropic effects. Also, they have been applied in various industrial applications, the cement paste being one example. The term thixotropy was originally coined to describe an isothermal reversible gel–sol (i.e. solid–liquid) transition due to mechanical agitation [3]. According to Barnes et al. [4], the accepted definition of thixotropy is "…a gradual decrease of the viscosity under shear stress followed by a gradual recovery of structure when the stress is removed…". Additional definitions of thixotropy are given in [5].

The amount of theoretical literature on the above mentioned time-dependent material is limited [4]. However, there is a comprehensive review article about the subject done by Mewis [3] and Barnes [5]. Also, a shorter review is given in Mujumdar et al. [6] and in a textbook by Tanner and Walters [7]. In these literatures, the various approaches used to measure thixotropy are presented. For example, one approach mentioned is by measuring the torque T under a linear increase and then decrease in angular velocity ω_o (of the rotating part of the viscometer). If the test sample is thixotropic, the two torque curves produced do not coincide, causing rather a hysteresis loop. While hysteresis loops are useful as a preliminary indicator of behavior, they do not provide a good basis for quantitative treatments [1,5]. However, an attempt can be made to quantify thixotropic behavior with such torque curve by its integration [1,5,8]. The use of this approach for SCC can for example be found in [9]. Another approach possible in studying thixotropic behavior is by monitoring the decay of measured torque from an initial value T_o to an equilibrium value T_e with time t, at a constant angular velocity ω_o (such an experiment can also be carried out when quantifying structural breakdown [1]). In some cases, simple exponential relationship can be found, but other and more complicated relationships can also exist. For example, Lapasin et al. [10] makes the use of the above approach on cement pastes, using three different types of functions, however more complicated

* Tel.: +354 5229000; fax: +354 5229311.
E-mail address: jon.wallevik@vvpf.net.

0008-8846/$ – see front matter © 2008 Elsevier Ltd. All rights reserved.
doi:10.1016/j.cemconres.2008.10.001

Nomenclature

3	the subscript 3 (as in X_3) designates the size 3 cement particles
4	the subscript 4 (as in X_4) designates the size 4 cement particles
a	parameter used in I_3 [–] (Eq. (9))
$\mathbf{g}$	gravity [m/s^2] (Eq. (29))
h	height of the inner cylinder = 116 mm (Sections 2 and 5)
H_3	coagulation rate [s^{-1}] (Eq. (7))
I_3	dispersion rate [s^{-1}] (Eq. (9))
I_3^s	dispersion rate (or rate of "break-apart") [s^{-1}] (Eq. (11))
I_4^s	dispersion rate (or rate of "break-apart") [s^{-1}] (Eq. (15))
J_3	number of reversible junctions per unit volume [m^{-3}] (Section 4.1)
J_3^s	number of reversible linkages per unit volume [m^{-3}] (Section 4.2)
$J_3^{p,c}$	number of permanent junctions per unit volume (Section 4.2)
$J_3^{p,s}$	number of permanent linkages per unit volume (Section 4.2)
J_3^p	number of permanent connections per unit volume = $J_3^{p,c}+J_3^{p,s}$ [m^{-3}] (Sections 4.1 and 4.2)
J_4^s	number of reversible linkages per unit volume [m^{-3}] (Section 4.3)
J_4^p	number of permanent linkages per unit volume [m^{-3}] (Section 4.3)
J_{tot}	total number of connections per unit volume [m^{-3}] (Section 4.3)
K	special function used in H_3 [s^{-3}] (Eq. (8))
n_3	number of primary particles per unit volume [m^{-3}] (Section 4.3)
n_4	number of primary particles per unit volume [m^{-3}] (Section 4.3)
$n_{3[t]}$	number of particles per unit volume [m^{-3}] (Eq. (1))
R	radial coordinate [mm] (Fig. 8)
R_i	radius of the inner cylinder = 85 mm (Section 2)
R_o	radius of the outer cylinder = 101 mm (Section 2)
t	time ($t\in$[0, 50 s]) (Figs. 4, 5 and 7)
t_m	time from water addition ($t_m\in$[0, 102 min]) (Section 2)
T	measured torque [Nm] (Figs. 4, 5 and 7)
T_c	computed torque [Nm] (Section 5; Figs. 4, 5 and 7)
U_3	reversible coagulated state = J_3/n_3 [–] (Eq. (27))
$U_{3[0]}$	reversible coagulated state at t = 0 [–] ($U_3\|_{t=0}=U_{3[0]}$)
U_3^s	reversible linked state = J_3^s/n_3 [–] (Eq. (26))
$U_{3[0]}^s$	reversible linked state at t = 0 [–] (Section 4.5.1)
U_4^s	reversible linked state = J_4^s/n_4 [–] (Eq. (28))
$U_{4[0]}^s$	reversible linked state at t = 0 [–] (Section 4.5.3)
$\mathbf{v}$	velocity of the cement paste [m/s] (Eq. (29))

Greek letters

α	parameter used in K [s$^{-2.99}$] (Eq. (8))
β	parameter used in K [s$^{-2.9}$] (Eq. (8))
$\dot{\gamma}$	shear rate [s^{-1}] (Section 5)
$\dot{\varepsilon}$	rate-of-deformation tensor [s^{-1}] (Section 5)
η	apparent viscosity (or equally, shear viscosity) [Pa·s] (Eq. (16))
κ	parameter used in I_3 [s^{a-1}] (Eq. (9))
λ	parameter used in I_3^s [s$^{-0.6}$] (Eq. (11))
μ	plastic viscosity [Pa·s] (Eq. (20))
$\tilde{\mu}$	thixotropic plastic viscosity [Pa·s] (Eq. (22))
$\hat{\mu}$	plastic viscosity of structural breakdown [Pa·s] (Eq. (24))
$\mu_{[t]}$	total plastic viscosity [Pa·s] (Eq. (18))
ξ_i	for i = I, III and V; material parameters used in Eqs. (22) and (24) [Pa·s]
ξ_j	for j = II, IV and VI; material parameters used in Eqs. (23) and (25) [Pa]
ρ	density of the cement paste [kg/m^3] (Eq. (29))
$\boldsymbol{\sigma}$	constitutive equation [Pa] (Section 5)
τ_0	yield stress (or equally, yield value; c.f. British Standard BS 5168:1975) [Pa] (Eq. (21))
$\tilde{\tau}_0$	thixotropic yield stress [Pa] (Eq. (23))
$\hat{\tau}_0$	yield stress of structural breakdown [Pa] (Eq. (25))
$\tau_{0[t]}$	total yield stress [Pa] (Eq. (19))
Φ	phase volume (i.e. solid concentration) of the cement paste [–] (Section 2)
χ	parameter used in I_4^s [s$^{-0.9}$] (Eq. (15))
ω_o	angular velocity of the outer cylinder (R_o) [rad/s] (Figs. 4, 5 and 7)

than of the simple exponential form. Nevertheless, as will be shown in Section 3, a material model created by this approach is limited because the apparent viscosity equation η can only be valid when a simple shear rate condition is applied to the rheological test. Considering an apparent viscosity equation extracted from such an experiment and then using it in another experiment of much more complicated shear history, would be almost impossible. For the latter case, at least the history of the shear rate must be included into the material model in one form or another.

Cheng and Evans suggested a general mathematical form of the equation of state for a thixotropic material, using a specific structural (or flocculation) parameter and a differential evolution equation to describe its time dependency [11]. An important property of such evolution equation is that it takes into account (in an implicit manner) the history of the shear rate. Based on the same approach as Cheng and Evans, Coussot developed a different thixotropic material model [12]. It proved able to describe cement based materials behavior when only submitted to short resting times [13]. Roussel improved this model in order to describe resting times longer than 1 min [14].

1.2. Structural breakdown

The term "structural breakdown" was made by Tattersall in 1954 [15]. Because no recovery in torque was measured in the corresponding experiment, structural breakdown was considered to be a different phenomenon than thixotropic behavior. The mechanism of structural breakdown was explained in 1983 in a textbook by Tattersall and Banfill [1]. There, it was attributed to the process of breaking certain linkages between the cement particles, which were assumed to be formed by the hydration process. The breaking of linkages was considered to be an irreversible process and thus non-thixotropic (the mechanism of structural breakdown will be further explained in Section 4.2).

In the earlier work of Wallevik [16,17], the use of a certain flocculation parameter was used, named "coagulated state". Rather than being based on a differential evolution equation, fading memory integrals of shear rate was used (i.e. the shear rate history was explicitly included into the calculations). This particular model was not based on the structural breakdown phenomenon, but rather on thixotropic behavior. More precisely, it was based on several ideas proposed by Hattori and Izumi [18] (an older reference to the work of Hattori and Izumi is available in [19]). However, with a purely thixotropic characteristic, the model was only partly successful. As will be explained in Section 4, the new model presented here will contain both the structural breakdown phenomenon and thixotropic behavior. With these two phenomena simultaneously present, a better outcome is attained (shown in Section 6). Due to programming complexity and longer calculation time, the use of fading memory integrals (as was done in [16,17]) is not applied in the new model presented here. Rather, the approach is using several connected differential evolution equations. A summary of these equations is given in Section 5.

2. Experimental

In this work, the rheological behavior of cement paste is analyzed by measuring torque $T(t)$ under complicated angular velocity $\omega_o(t)$ conditions, shown in Fig. 1b (as well as in Fig. 4a). The challenge is to create a material model that is based on the microstructural approach and is able to simulate the measured rheological behavior of the cement paste. The challenge is especially great when a complicated angular velocity is used in the experiment. With a good apparent viscosity function $\eta=\eta(\dot{\gamma},\ldots)$ used in the numerical simulation, the computed torque T_c should be able to overlap the measured torque T. The objective is that with such satisfactory material model, a better idea of what controls the rheological behavior of the cement based material can be presented.

2.1. Measuring device

The viscometer used is the ConTec Viscometer 4 [20,21]. It is a coaxial cylinders viscometer that has a stationary inner cylinder (of

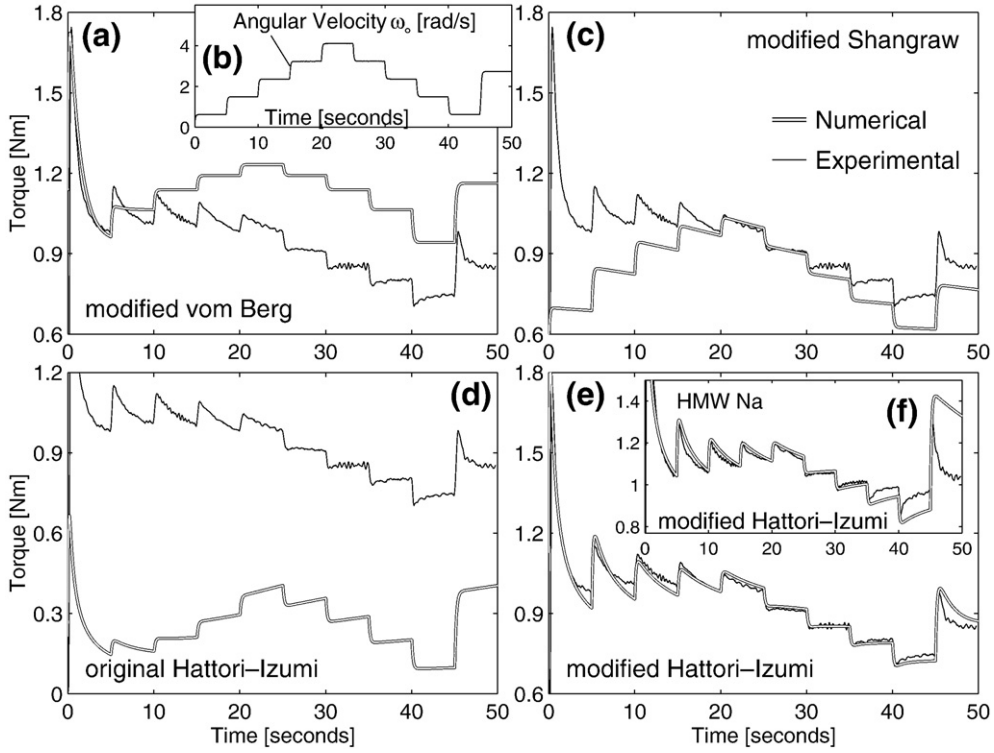

Fig. 1. The results from miscellaneous theories. Experimental data for illustrations (a) to (e) are from the SNF-case at t_m=72 min, while (f) is the HMW Na-case at t_m=72 min.

radius R_i=85 mm) that measures torque T, and a rotating outer cylinder (of radius R_o=101 mm) that rotates at predetermined angular velocities ω_o (shown in Figs. 1b and 4a). The height of the inner cylinder is h=116 mm. Shearing from the bottom part of the viscometer is filtered out by special means [20,21]. To avoid slippage between the cylinders and the cement paste, both the inner and outer cylinders are fitted with (small sized) protruding vanes [22,23]. With this, the dimensions R_i and R_o are relative to the extremities of the vanes. For a viscoplastic material, it is assumed that the material is held in the space between the vane blades so that the material and the vanes together behave like a rigid cylinder. Experimental observation supports this assumption and is in accordance with the findings made in [24] (see also [25,26]). Hence, any attempt to investigate the flow between the vane blades is not done in this work.

2.2. Admixture

Three different types of admixtures are used. These are superplasticizers and are designated as VHMW Na, HMW Na and SNF, respectively. The first two are a very high- and a high molecular weight Na-lignosulfonates, respectively. These are natural polymers formed from the pulping process and are produced by Borregaard LignoTech, Norway. The SNF is a sulfonated naphthalene-formaldehyde condensate polymer and is synthetically formed. It has the commercial name Suparex M40 and is produced by Hodgson Chemicals Ltd. More information about the properties of these superplasticizers can be found in [17].

2.3. Mix design of the cement paste

The mass ratio of water to cement for the cement paste is w/c=0.3 and the amount of superplasticizer used is 0.5% solid by weight of cement. The initial phase volume (i.e. solid concentration) is equal to Φ=0.52 and is always increasing with time due to the hydration of the cement particles [16]. As is well known, hydration is a reaction of an anhydrous compound (i.e. cement particles) with water, yielding a new compound, a hydrate. The hydrate quickly covers the cement particle surface (i.e. a hydrate membrane is formed) to increase the surface roughness and the phase volume, giving a certain increase in the apparent viscosity η with time t_m.

2.4. Mixing procedure

A Hobart AE120 mixer is used when mixing the cement paste. It has three speed settings for the agitator and the attachment (i.e. the whips), respectively: Speed 1: 106 and 61 rpm, Speed 2: 196 and 113 rpm and Speed 3: 358 and 205 rpm. The agitator rotates clockwise and the attachment rotates counterclockwise. The attachment is blade shaped, like an open shield. The cement (in dry condition) is first placed into the mixing bowl (at zero speed). Thereafter, the water is poured into the bowl during mixing at speed 1. The time t_m=0 min marks the initial water addition to the cement (the subscript "m" is an acronym for "mixing"). Prior to this the water is premixed with either lignosulfonate or SNF polymer. The mixing procedure for the cement paste is a four-step procedure: (1) Mixing of cement and water at Speed 1 ($t_m \in$[0 min, 3 min]). (2) Hand mixing to break up clumped cement particles ($t_m \in$[3 min, 6 min]). (3) Mixing at Speed 2 ($t_m \in$[6 min, 10 min]). (4) Check with hand mixing if the suspension is homogeneous ($t_m \in$[10 min, 11 min]). The first viscometric measurement occurs at t_m=12 min.

2.5. Measuring procedure

At t_m=12, 42, 72 and 102 min after the initial water addition, a measurement with the viscometer is performed. Each measurement takes 50 s. Immediately after each such test, a remixing by hand is done to ensure homogeneity. Thereafter, the test material is at rest until the next measurement (about 29 min). It should be noted that the Hobart mixer is only used once for each batch. More precisely, it is only used during the first 10 min of each experiment as described in Section 2.4.

3. The need for an improved model

The angular velocity ω_o used in a single rheological test is shown in Fig. 1b. An example of experimental result by such rotation is shown in Fig. 1a–e, and are from the SNF-case at t_m=72 min. This is the same data as shown later in Fig. 5c (Section 6.2). For Fig. 1f, then a different polymer is used, namely the HMW Na and the result applies at t_m=72 min as well. This is the same data as shown in Fig. 7c (Section 6.3).

Using classical models like that of the modified vom Berg [10], or of the modified Shangraw [10] to fit the experimental data in Fig. 1 is unattainable. Their primary failure rests in the way these models are generated, namely from an experiment where simple angular velocity condition is applied to the rheological test. Using such simple test setup makes it that much easier to fit the experimental data to whatever model one chooses.

Fig. 1a is adopted from [27] and shows an attempt to fit the modified vom Berg model to the experimental data. The model modification is done by Lapasin et al. [10]. For this case, by setting the material parameters to such that it simulates the first part of the experimental data, the rest of the experimental data cannot be simulated. A wide variety of different parametric values were tested by trial and error, without any success. The same applies for the modified Shangraw model, shown in Fig. 1c (adopted from [27]). There, an attempt is made to fit the middle part of the experimental data as much as possible. However, with the material parameters fixed with that objective, the rest of the experimental data cannot be simulated.

Using the original Hattori–Izumi theory [18] was also shown to be unattainable. This is shown in Fig. 1d (adopted from [27,17]). One of the problems of this theory is that it does not include a yield stress, which means that the computed torque cannot be elevated to the "height" where the experimental data is. The other problem with this theory is that in the limit $t \to \infty$, the output of the corresponding algebraic evolution equation is a constant regardless of how much shear rate $\dot{\gamma}$ or coagulation rate H is present; i.e. under sufficiently large value of time t, it overshadows all physical processes described by the shear rate $\dot{\gamma}$ and the coagulation rate constant H. This particular behavior is well explained in [16] (Section 3.4).

Fig. 1e shows the result of using the MHI-theory (i.e. the modified Hattori–Izumi theory) and is adopted from [16,17]. As shown, this model is successful for the SNF-case. However as shown in Fig. 1f, when using the HMW Na polymer in the cement paste, a worse result is attained. The problem is apparently present in its failure to reproduce the large recovery in the measured torque. Accordingly, the MHI-theory has its limitations.

In the remainder of this work, a new theory is presented, in which the problems presented in Fig. 1 are solved. For lack of better term, the theory is designated as the *Particle Flow Interaction Theory* (or the PFI-theory). Its current version is labeled as "Mark I" (future developments will be labeled Mark II, Mark III, and so forth). As will be clear in Section 6, the current version of the PFI-theory (i.e. Mark I) has some unresolved issues (see for example Fig. 6), but still is an important improvement over the MHI-theory and this is the main objective of the current work.

4. Types of particle interactions during the flow of cement particles

The PFI-theory (Mark I) is based on several ideas proposed by Hattori and Izumi [18] and by Tattersall and Banfill [1]. More precisely, coagulation, dispersion and re-coagulation of the cement particles in

combination with the breaking of certain chemically formed linkages between the particles are assumed to play an important role in generating the overall time-dependent behavior of the cement paste. What now follows are explanations of the two basic concepts, the new proposed supplements and how all these ideas are combined and implemented by mathematical means.

4.1. Reversible and permanent junctions

In [16,17], the thixotropic behavior of cement paste is related to coagulation, dispersion and re-coagulation of the cement particles. This is in accordance with the original idea presented by Hattori and Izumi [18]. Here, the term "coagulation" appears frequently and it describes the occurrence when two (or more) cement particles come into a contact with each other for some duration of time; i.e. when the cement particles become "glued" to each other and work is required to separate them. The particles become glued together as a result of the total potential energy interaction that exists between them. It originates from combined forces of van der Waals attraction, electrostatic repulsion and steric hindrance [1,17,28]. The polymers mentioned in Section 2.2 will generally adsorb on the surface of the cement particles. Their function is to change the above mentioned total potential energy in such manner that coagulation is more difficultly obtained and dispersion more easily achieved.

In addition to the original theory [18], it is proposed in [16,17] that there are basically two kinds of coagulation. The first type is the reversible coagulation, where two coagulated cement particles can be separated (i.e. dispersed) again by the given rate of work available to the suspension (the rate of work is provided by the engine of the viscometer). The second type of coagulation is the permanent coagulation, where the two cement particles cannot be separated by the given rate of work (i.e. power) available. The simultaneous presence of both permanently- and reversibly coagulated cement particles in the cement paste, could for example be attributed to damaged (and therefore non-functional) polymers between some cement particles, and to still very functional polymers between other cement particles, respectively.

The connections (or contacts) between the cement particles, formed by the total potential energy interaction, are named *junctions*. The number of *reversible junctions* (from the process of reversible coagulation) is represented with the term J_3 (previously designated as J_t in [16,17]). Likewise, the number of *permanent junctions* (from permanent coagulation) is designated with J_3^p (previously designated as J_t^p in [16,17]). The superscript "p" is an acronym for "permanent", or more precisely "permanent coagulation" (and "permanent linking", as explained below).

4.2. Breakable and permanent linkages

Within a few seconds of the initial contact between cement and water, the surfaces of the cement particles are covered by a membrane of gelatinous calcium silicate/sulphoaluminate hydrate [1]. Hence in [1,8], it is suggested that when a pair or more, of cement particles come into contact with water, this hydrate membrane forms around both of them. As soon as the cement paste is agitated, the linkages between the cement particles may be broken [1]. That is, the bridging membrane ruptures and the cement particles separate. As no recovery of structure was measured for such cases (i.e. is an irreversible process), the term "structural breakdown" was preferred over "thixotropic behavior" [1,8,15,29,30]. The notion of linkages between cement particles was first proposed by Tattersall [30].

In this work, it is assumed that there are basically two kinds of bridging membranes. The first type is the breakable membrane, where two linked cement particles can be broken apart (i.e. dispersed) by the given rate of work available to the suspension. The second type of bridging membrane is the permanent membrane, where the two linked cement particles cannot be broken apart with the given power available. The strength of the link between two (or more) cement particles depends on the thickness of the membrane around them and contact geometry [1]. Hence, with different conditions between different cement particles, it is not hard to imagine a simultaneous presence of both permanently- and breakable linked cement particles in the cement paste.

As indicated above, the connections (or contacts) between the cement particles, formed by the hydrate membrane, are named *linkages*. The number of *breakable linkages* (by the formation of breakable weak/thin hydrate membrane) is represented with the term J_3^s (the superscript "s" is an acronym for "structural breakdown"). Likewise, the number of permanent linkages (by the formation of permanent strong/thick hydrate membrane) is designated with J_3^p.

Regardless if the cement particles are permanently coagulated (by the total potential energy) or permanently linked (by the hydrate membrane), these two contributions are represented with the same symbol, namely with J_3^p. For example, if two cement particles are permanently coagulated (giving $J_3^{p,c}=1\ m^{-3}$), and another pair of cement particles are permanently linked (giving $J_3^{p,s}=1\ m^{-3}$), the total value of J_3^p is $J_3^{p,c}+J_3^{p,s}=2\ m^{-3}$. That is, to simplify the presentation, no distinction is made between coagulated- and linked cement particles when they are permanently connected.

From the above text and from Section 4.1, the total number of connections between coagulated- and linked cement particles of size 3 is $J_3+J_3^s+J_3^p$.

4.3. Particle size numbers 3 and 4

Cement particles are poly-dispersed in size. Some 7–9% of the material (by weight) is typically finer than 2 μm in diameter and 0–4% coarser than 90 μm [31]. Traditionally, the particles that are influenced by the total potential energy effects (see Section 4.1) are considered to be colloid particles. General definition of such particle is that at least one dimension is in the size range from 1 nm to 1 μm [28,32]. However, there is no clear distinction between the behavior of particles with somewhat larger dimensions than those of the traditional colloidal particle [28]. In [17] (Section 2.5.2), it is demonstrated that cement particles as large as 40 μm in diameter seem to be able to "behave", at least to some degree, as a colloid particle, somewhat controlled by the action of the total potential energy. All cement particles (i.e. the domain of particle sizes) that can significantly be influenced by the total potential energy effects are classified in this work as "particle size number 3" (meaning that the diameter of these particles is less than the above mentioned 40 μm).

When considering a pair of cement particles larger than of "particle size number 3", their kinetic energy (or inertia) starts to be sufficiently large to overcome their mutual energy barrier against coagulation and dispersion. When this condition applies, coagulation does not occur and the cement particles rather interact with each other by a pure hard sphere collision factor. Such cement particles that are not (or only slightly) influenced by the total potential energy effects, are classified here as "particle size number 4". As cement particles of this size domain do not coagulate, the corresponding (reversible) junction number is always zero, meaning $J_4=0\ m^{-3}$. However, as it is fair to assume that the cement particles of size 4 are covered by a hydrate membrane, just as for size 3, the values of J_4^s (breakable linkages) and J_4^p (permanent linkages) do not have to be zero.

In [18], the subscripts "1" and "2" (giving J_1 and J_2) are reserved for water molecules and water adsorption. It is therefore for historical reason that it is started here with the subscript "3" for the smaller cement particles, and thereafter with "4" for the larger cement particles.

From the above text and from Sections 4.1 and 4.2, the total number of connections between coagulated and linked cement particles of size 3 and 4 is $J_{tot}=J_3+J_3^s+J_3^p+J_4^s+J_4^p$. The variables J_{tot}, J_3,

J_3^s, J_3^p, J_4^s and J_4^p are so-called *direct microstructural parameters*, with the physical unit of [m^{-3}]; i.e. these terms represent the number of connections per unit volume. In either case of reversible coagulation/linking or of permanent coagulation/linking, the effect to the apparent viscosity η is basically the same, namely to increase its value. In [17] (Section 2.4.1), the apparent viscosity η is roughly calculated by using Bagnold's original theory [33] about particle–particle interaction (i.e. rate of momentum transfer between particles). There, it is clearly demonstrated how increased J_{tot} value increases the apparent viscosity η.

For size 3 cement particles, two types of primary particles (i.e. cement particles) are defined. One is primary particles that will undergo a reversible coagulation and linking and is designated with n_3. The other type is primary particles that will undergo a permanent coagulation and linking and is represented with n_3^p. The physical unit of n_3 and n_3^p is in [m^{-3}], meaning number of primary particles per unit volume. As discussed in [16] (Section 3.4.2), when considering cement based materials, the number of primary particles is slowly changing with time. However, relative to a single experiment of 50 s (see Section 2.5) n_3 and n_3^p (as well as n_4 and n_4^p for size 4) can safely be considered as constants.

Fig. 2 gives a summary of the different types of connections that are assumed to be present in the cement paste. In Fig. 2a, is a realistic presentation of cement paste, and in Fig. 2b is a magnification of some part of it (an idealized representation). For this last mentioned illustration, there is also shown the number of corresponding connections J (units not shown). In Fig. 2c is shown a reversible linkage between two size 4 cement particles.

When examining Fig. 2b, it should be clear that in the current version of the PFI-theory, no explicit assumption is made about the shape of the cement particles. For example, going from spherically shaped cement particles in one batch, to cubically shaped cement particles in another batch, will only reflect in larger values in some of the material parameters of the model. Hence, the shape of the particles is only reflected in changed values for some of the material parameters used in the PFI-theory. The same consideration applies for the surface roughness of the cement particles.

From the above text, an *indirect microstructural parameter* can be defined as $U_3=J_3/n_3$, $U_3^s=J_3^s/n_3$ and $U_3^p=J_3^p/n_3^p$. In the same fashion, for size 4 cement particles, then $U_4^s=J_4^s/n_4$ and $U_4^p=J_4^p/n_4^p$. As explained in [16] (Section 3.2), the indirect microstructural parameter can generally have values ranging from 0 to 1. There is however now a specific restriction to this as explained later in Section 4.5.1. The term U_3 will be referred to as the (reversible) coagulated state. Likewise, the two terms U_3^s and U_4^s will be referred to as (reversible) linked state.

The issue of cement particles, of different size domain, connecting to each other, i.e. U_{34} U_{34}^s and U_{34}^p is not implemented in the current version of the PFI-theory, but is briefly discussed in Section 7.2.

4.4. Implementation of thixotropic behavior

4.4.1. Particle size number 3

In [18], the perikinetic coagulation rate theory established by Verwey and Overbeek [34] is employed (perikinetic means without stirring $\dot{\gamma}=0$, while orthokinetic means with stirring $\dot{\gamma}>0$). This theory is used here for the cement particles of size 3, which can coagulate and disperse as explained in Section 4.1. Hence, the decrease in number of particles $n_{3[t]}$ in the suspension is expressed with Eq. (1) (the concept of number of particles $n_{3[t]}$ versus the number of primary particles n_3 is for example explained with Fig. 2 in [16])

$$-\frac{dn_{3[t]}}{dt}=\frac{H_3 n_{3[t]}^2}{n_3}. \tag{1}$$

In the above equation, the term H_3 is the coagulation rate for cement particles of size 3, and has the physical unit of [1/s] (previously designated as H in [16,17]). In [16,17,18], the following relationship is shown to apply

$$n_{3[t]}=n_3-J_3. \tag{2}$$

Using the above equation with $J_3=n_3U_3$ and n_3=constant (see Section 4.3) in Eq. (1), the following is obtained

$$-\frac{dn_{3[t]}}{dt}=-\frac{d(n_3-J_3)}{dt}=\frac{dJ_3}{dt}=n_3\frac{dU_3}{dt} \tag{3}$$

$$\frac{H_3 n_{3[t]}^2}{n_3}=H_3\frac{(n_3-J_3)^2}{n_3}=H_3\frac{n_3^2(1-U_3)^2}{n_3}. \tag{4}$$

Combining the two above equations (c.f. Eq. (1)), with the inclusion of a dispersion function $f=f(I_3,J_3,n_3)$ and thereafter dividing by n_3, gives

$$\frac{dU_3}{dt}=H_3(1-U_3)^2-\frac{f(I_3,J_3,n_3)}{n_3}. \tag{5}$$

The function f in the above must be included to allow the coagulated state U_3 to decrease, which then would correspond to dispersion of the cement particles. The best computational result was obtained by using $f(I_3J_3,n_3)/n_3=I_3(\dot{\gamma})U_3^2$. The term I_3 is the dispersion rate for cement particles of size 3, and has the physical unit of [1/s]

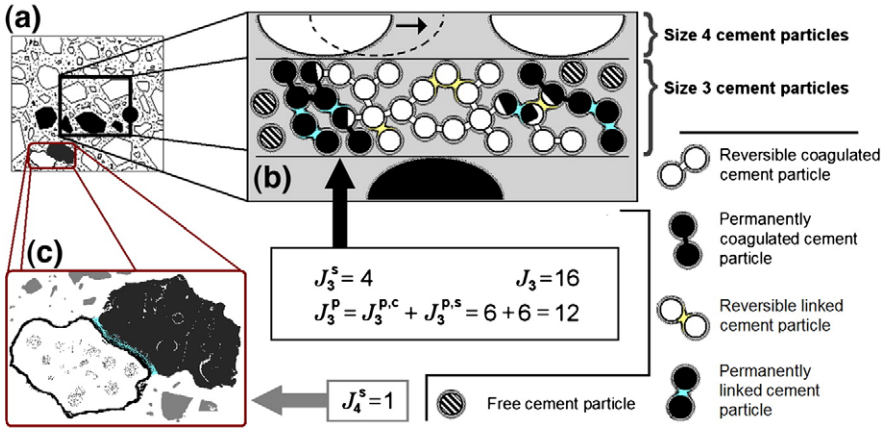

Fig. 2. A summary of the different types of connections that are assumed to be present in the cement paste (permanent linkages of size 4 cement particles are not shown).

(previously designated as I in [16,17]). With this, Eq. (5) is transformed into

$$\frac{dU_3}{dt} = H_3(1-U_3)^2 - I_3 U_3^2. \quad (6)$$

It is interesting to note that in its current state, the above equation starts to resemble a specific balance equation discussed by Mujumdar et al. [6]. However, since both linked- and coagulated cement particles share the same set of primary particles n_3, the above equation is not complete. Its final form is shown with Eq. (13) (see also Eq. (12)).

In the original Hattori–Izumi theory [18], it is assumed that the total number of junctions J_3 increases by a naturally occurring perikinetic coagulation process only. In other words, it is assumed that the coagulation rate H_3 exists only because of the Brownian motion of the cement particles. However, as discussed in [28], the coagulation rate H_3 is greatly influenced by the stirring of the suspension. The stirring causes the particles to be thrown together at a larger rate than the normal diffusion rate and hence the orthokinetic processes increase coagulation. An explanation of the problem is given by Smoluchowski and is reproduced in [28]. There it is shown that the orthokinetic process becomes increasingly important with increasing particle size. With larger particles, such as in emulsions (droplet diameter $\propto 10^{-7}$ m), orthokinetic coagulation can occur up to as much as 10^4 times the perikinetic rate [32]. With particles at the lower end of the colloidal size range (diameter $\propto 10^{-9}$ m), stirring has relatively little effect on their rate of coagulation [32]. Since non-hydrated cement particles can be up to and larger than $90\cdot10^{-6}$ m in diameter [31], the orthokinetic coagulation process plays an important role in determining the correct coagulation rate H_3 and hence in determining the correct coagulated state U_3.

According to the above paragraph, the stirring causes the cement particles to be thrown together at a larger rate than the normal diffusion rate. Hence, it is to be expected that the condition $dH_3/d\dot{\gamma} \geq 0$ applies for all $\dot{\gamma} \geq 0$. However, it can be argued that with continuously increasing shear rate $\dot{\gamma}$, the mutual kinetic energy of two cement particles that are about to collide, will also increase in the process. There will come a condition (designated with $\dot{\gamma}_{cr}$) where this kinetic energy is sufficient to overcome the potential energy barrier that can hold them together in a coagulated state. The rate of collisions between the cement particles will always increase with increasing shear rate $\dot{\gamma}$. However, beyond the point of $\dot{\gamma}_{cr}$ fewer and fewer of these collisions will result in actual coagulation. This means that the coagulation rate will start to decrease with further increase in shear rate, meaning $dH_3/d\dot{\gamma} \leq 0$ for all $\dot{\gamma} \geq \dot{\gamma}_{cr}$. The coagulation rate equation used in this work holds the overall above mentioned properties and is given by

$$H_3 = \frac{K}{\dot{\gamma}^2 + l} \quad (7)$$

where

$$K = \left(\alpha\dot{\gamma}^{0.01} + \beta\dot{\gamma}^{0.1}\right)e^{-\zeta(\partial\dot{\gamma}/\partial t)^2} + K_0. \quad (8)$$

The terms l, ζ and K_0 are empirical constants, kept equal to $l = 10\ s^{-2}$, $\zeta = 4\cdot10^{-4}\ s^4$ and $K_0 = 10^{-4}\ s^{-3}$ at all times (previously in [16,17], the value $l = 1\ s^{-2}$ was used). In [16,17], the function K was a step function that increased and decreased parallel to $d\omega_o/dt$. As shown above, this is no longer the case as K now only depends on intrinsic variables, namely on the shear rate $\dot{\gamma}$ and its time derivative $\partial\dot{\gamma}/\partial t$. At $\dot{\gamma} = 0$, then $H_3 = K_0/l = 10^{-5}\ s^{-1}$, which is the coagulation rate induced by the Brownian motion of the cement particles (i.e. coagulation induced only by the naturally occurring perikinetic processes).

The best computational result was obtained by using the following dispersion rate function

$$I_3 = \kappa\dot{\gamma}^a. \quad (9)$$

Although determined by empirical means, the material parameters in Eqs. (7)–(9) depend, among other factors, on the total potential energy interaction between the cement particles.

4.5. Implementation of structural breakdown

4.5.1. Particle size number 3

When forming an equation for the linked state U_3^s of size 3 cement particles (see Section 4.2), the basis is taken from Eq. (6). Hence at first consideration, it could be written as $dU_3^s/dt = H_3^s(1-U_3^s)^2 - I_3^s[U_3^s]^2$. As the reformation of linkages is very slow (or perhaps not occurring at all) relative to the experiment of 50 s, the value of H_3^s can be set as zero. Furthermore, the best computational result was obtained by dropping the exponent of "2" in the "$-I_3^s[U_3^s]^2$" part. With this, the equation describing the structural breakdown for size 3 cement particles becomes

$$\frac{dU_3^s}{dt} = -I_3^s U_3^s. \quad (10)$$

In the above equation, the term I_3^s is the rate of "break-apart" function. That is, it describes the rate at which the linkages between the size 3 cement particles are broken apart (see Section 4.2) and has the physical unit of [1/s]. To simplify, it will also be designated as dispersion rate (i.e. it will have the same designation as I_3 in Eq. (6)). The best outcome was obtained by using the following function

$$I_3^s = \lambda\dot{\gamma}^b. \quad (11)$$

The term b is set equal to 0.4 at all times, while λ is generally changing from one experiment to the next.

4.5.2. Constraints of structural breakdown and thixotropic behavior

As explained in [16] (Section 3.2), the value of coagulated state U_3 for size 3 cement particles generally range from 0 to 1. With $U_3 = 0$, no cement particles are coagulated and the number of particles $n_{3[t]}$ is equal to the number of primary particles n_3 (shown with Fig. 2a in [16]). With $U_3 = 1$, all the primary particles are coagulated and the number of particles is $n_{3[t]} = 1\ m^{-3}$ (shown with Fig. 2c in [16]). However, when adding the concept of linked cement particles (and hence, linked state U_3^s) into the physical infrastructure, the maximum coagulated state U_3 can no longer be as large as 1. This is because some of the size 3 cement particles can already be occupied in a linked state (i.e. are connected by the hydrate membrane and not by the total potential energy). More precisely, as all size 3 cement particles that can either be reversibly linked or reversibly coagulated, together define the number of primary particles n_3, it is only the value of $U_3 + U_3^s$ that can reach 1. With this, the maximum value for U_3 is now $1 - U_3^s$. Of course, the same condition must apply for the initial condition of U_3 and U_3^s. That is, the maximum value of the sum $U_3|_{t=0} + U_3^s|_{t=0} = U_{3[0]} + U_{3[0]}^s$ is 1, while the minimum value is 0.

Fig. 3 gives an additional explanation to the above paragraph. In this example are two illustrations (a) and (b) of the same set of cement particles. Hence, the number of primary particles is $n_3 = 21\ m^{-3}$ in both cases. Also, in both illustrations, the number of linkages is the same or $J_3^s = 5\ m^{-3}$, meaning $U_3^s = J_3^s/n_3 = 5/21 = 0.238$. In illustration (a) the number of junctions is $J_3 = 0\ m^{-3}$. Because some of the cement particles are already occupied in a linked state ($J_3^s = 5\ m^{-3}$), the coagulated state U_3 cannot reach 1 in illustration (b), but only $U_3 = J_3/n_3 = 15/21 = 0.714$.

Since all cement particles are connected in Fig. 3b, the value of $U_3 + U_3^s$ should ideally be equal to 1. It is however 20/21 = 0.952 and is just a consequence of the very few cement particles treated in this simple example.

From a strict mathematical point of view, the role that the "$(1-U_3)^2$" part plays in Eq. (6) is to stop coagulation when the value of U_3 has reached 1. For such case, the term "$H_3(1-U_3)^2$" becomes zero, and U_3 can at that moment only decrease through the "$-I_3U_3^2$" part in Eq. (6).

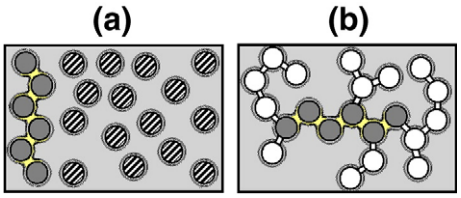

Fig. 3. Illustration of why the maximum value of U_3 cannot reach 1 when $U_3^s \neq 0$. For both illustrations: $n_3 = 21\ m^{-3}$; $J_3^s = 5\ m^{-3}$. For illustration (a): $J_3 = 0\ m^{-3}$, while for (b): $J_3 = 15\ m^{-3}$.

From the above text, it is clear that the "$H_3(1-U_3)^2$" part must be transformed to "$H_3([1-U_3^s]-U_3)^2$", inhibiting U_3 to grow beyond $1-U_3^s$ (that is, inhibiting $U_3+U_3^s$ to grow beyond 1). With this change, Eq. (6) is transformed to

$$\frac{dU_3}{dt} = H_3\left([1-U_3^s]-U_3\right)^2 - I_3 U_3^2. \tag{12}$$

As U_3^s decreases (by Eq. (10)), the term $1-U_3^s$ increases, which again results in that the potential maximum value of U_3 is increased (by Eq. (12)). For example, if U_3^s decreases from 0.748 down to 0.358, then $1-U_3^s$ is increased from 0.252 up to 0.642, meaning that the term $H_3([1-U_3^s]-U_3)^2 = H_3(0.642-U_3)^2$, won't become zero until U_3 has reached 0.642. More precisely, the maximum value for U_3 is increased up to 0.642 (from the previous value of 0.252). To summarize: A reduction in U_3^s (then always by Eq. (10)), corresponds to that linked cement particles are broken apart. This reduction also results in a larger potential maximum value for U_3 (by Eq. (12)), which must correspond to an increased number of cement particles available to participate in coagulation. That is, when linked cement particles are broken apart, then according to Eq. (12), they become available to participate in coagulation.

In the spirit of the original theory [1,8,29] about "no recovery of structure" (see the first paragraph in Section 4.2), it will be assumed that linked cement particles that are broken apart will not coagulate, at least not during the short time interval of 50 s, while an experiment is occurring. More precisely, cement particles with broken linkages are not allowed to participate in the process of coagulation, dispersion and re-coagulation (i.e. participate in thixotropic behavior) during the time interval of 50 s. To accommodate this concept, the variable U_3^s in Eq. (12) is frozen to its initial value $U_3^s|_{t=0} = U_{3[0]}^s$, giving the following equation

$$\frac{dU_3}{dt} = H_3\left(\left[1-U_{3[0]}^s\right]-U_3\right)^2 - I_3 U_3^2. \tag{13}$$

With $1-U_{3[0]}^s$ as a constant, the maximum value for U_3 becomes also a constant, meaning that the number of cement particles available to participate in coagulation is always the same (i.e. no new particles become available during a single rheological test lasting 50 s). Allowing the cement particles with broken linkages to participate in the process of coagulation, dispersion and re-coagulation (i.e. using Eq. (12) without changes), is considered for future work (then designated as the PFI-theory, Mark II).

4.5.3. Particle size number 4

When forming the equation for the linked state U_4^s of size 4 cement particles (i.e. of the larger cement particles, c.f. Section 4.3), the basis is taken from Eq. (10), giving

$$\frac{dU_4^s}{dt} = -I_4^s U_4^s. \tag{14}$$

The rate of "break-apart" function for the size 4 cement particles (also designated as dispersion rate) is based on Eq. (11) and is given by

$$I_4^s = \chi \dot{\gamma}^c. \tag{15}$$

The term c is set equal to 0.1 at all times, while χ is generally changing from one experiment to the next.

As the primary particles n_4 are only associated with linked cement particles and not with coagulated particles (since coagulation cannot occur for this size domain, c.f. Section 4.3), the value of U_4^s ranges from 0 to 1. That is, the restriction that applies for U_3 and U_3^s, does not apply for U_4^s.

4.6. Viscoplastic material behavior

As applies in [16], the material behavior of the cement paste is of viscoplastic character, here described with

$$\eta = \mu_{[t]} + \frac{\tau_{0[t]}}{\dot{\gamma}}, \quad \tau \geq \tau_{0[t]} \tag{16}$$

$$\dot{\gamma} = 0, \qquad \tau < \tau_{0[t]} \tag{17}$$

where τ is the shear stress. The computational implementation of Eqs. (16) and (17) is done through the regularization approach [35–38]. The terms $\mu_{[t]}$ and $\tau_{0[t]}$ are the "total" plastic viscosity and the "total" yield stress, and are defined by the two following equations

$$\mu_{[t]} = \mu + \tilde{\mu} + \hat{\mu} \tag{18}$$

$$\tau_{0[t]} = \tau_0 + \tilde{\tau}_0 + \hat{\tau}_0. \tag{19}$$

The value of $\tau_{0[t]}$ at $t=0$ can be designated as static yield stress and its significance is for example explained in [17] (Section 3.2.2), as well as in [2] ("Paper 5").

According to [16] (Section 3.4.2), the existence of plastic viscosity μ and yield stress τ_0 are related to two processes (see also pp. 26–28 in [17] about the following issue). The first process is a certain basic minimum particle–particle interaction between unconnected cement particles (i.e. rate of momentum transfer between "free" cement particles). The second process is the increased interaction between all cement particles as a result of permanent coagulation $J_3^{p,c}$. Here, it will be assumed that permanently linked cement particles of size 3 and 4 (that is, $J_3^{p,s}$ and J_4^p) play also a role in μ and τ_0, just as permanent coagulation $J_3^{p,c}$ does. With $U_3^p = (J_3^{p,c}+J_3^{p,s})/n_3^p$ and $U_4^p = J_4^p/n_4^p$ (see Sections 4.2 and 4.3), this means

$$\mu = \mu\left(U_3^p, U_4^p, \ldots\right) \tag{20}$$

$$\tau_0 = \tau_0\left(U_3^p, U_4^p, \ldots\right). \tag{21}$$

Most certainly, the above depends also on other factors like the surface roughness of the cement particles, solid concentration Φ, particle shape and hydrodynamic effects (if present at relevant magnitude).

The thixotropic plastic viscosity and yield stress have the same form as presented in [16],

$$\tilde{\mu} = \xi_I [U_3]^q \tag{22}$$

$$\tilde{\tau}_0 = \xi_{II} [U_3]^r. \tag{23}$$

The plastic viscosity and yield stress of structural breakdown are based on a similar relationship as shown above, given by

$$\hat{\mu} = \xi_{III} \left[U_3^s\right]^q + \xi_V U_4^s \tag{24}$$

$$\hat{\tau}_0 = \xi_{IV} \left[U_3^s\right]^r + \xi_{VI} U_4^s. \tag{25}$$

Although determined by empirical means, the six terms ξ_I to ξ_{VI} are material parameters depending, among other factors, on the surface roughness of the cement particles, particle shape and solid

concentration Φ. The term r is equal to 2/3 at all times and is in accordance with the original theory [18]. For most cases, the same applies for the term q. The exception is the HMW Na-case in Section 6.3, where q is set equal to 1/2 at t_m=42, 72 and 102 min, as this gave a better outcome.

Here, it is assumed that the reformation of hydrate membrane can occur for the same batch at later time. The reason for this reformation could be related to the particular cement- and admixture type used here in combination with sufficiently long resting time of 29 min between two measurements (see Section 2). More precisely, half an hour might be long enough for allowing subsequent reformation of new hydrate membrane around then already connected cement particles, which then ruptures in the next experiment and hence is registered as new/additional structural breakdown in the measurement. This means that the values $\hat{\mu}$ and $\hat{\tau}_0$ are generally non-zero at later experiments t_m=42, 72 and 102 min. Suffice to say, it was necessary to allow for this to gain a successful computational outcome.

4.7. The simultaneous presence of junctions and linkages

From Sections 4.1–4.3, it is clear that the PFI-theory works simultaneously with two different types of connections, namely junctions and linkages. Since the formation of linkages depends on chemical reactions, it is not as spontaneous process as the formation of junctions. Also, to make the formation of linkages possible, the size 3 cement particles must be coagulated together during the reactions. For the larger cement particles (i.e. of size 4) the same type of condition must apply. That is, they must be connected together during the reactions, then not by coagulation but rather by some sort of inertial based process (for example by the combination of lack of space in the paste ($\Phi \geq 0.52$, c.f. Section 2) and a slight settlement induced by gravity). Hence, during the resting time of 29 min, two (or more) connected cement particles will try to form a (reversible or permanent) link. Whether the hydrate membrane will result in a particular link formation or not, will most likely depend on conditions like what mineral types are adjoined to each other for two connected cement particles (i.e. alite, belite, aluminate or ferrite), thickness of the adsorbed polymer in between, contact angle and surface roughness of the mineral in question and of its already developed hydrate. For example, in the case when the layer of polymers is sufficiently thick between two size 3 cement particles, it should prevent a link formation, allowing them to remain in a coagulated state during the resting time of 29 min. In the neighboring pair (of size 3), such thickness could be too small, meaning a successful link formation would occur for that case. The idea here is that it is the severe heterogeneity of the cement particles (and of the polymer (see [17], Section 4.4.2), including its different degree of affinity to the particular mineral type (see [17], Section 6.4.1)) that actually allow for a simultaneous presence of both junctions and linkages in the cement paste. Regardless whether the above idea is valid or not, then it should be clear that it is imperative to allow for the simultaneous presence of junctions and linkages (by Eqs. (26)–(28)) to make the overall computational result successful.

5. System of equations

Before going into the main results in Section 6, it is prudent to summarize the system of equations that is used in the PFI-theory.

With $\mathrm{d}/\mathrm{d}t=\partial/\partial t+\mathbf{v}\cdot\nabla$ (see for example [17], Section 2.2), then Eqs. (10), (13) and (14) becomes

$$\frac{\partial U_3^s}{\partial t}+\mathbf{v}\cdot\nabla U_3^s=-I_3^s U_3^s \tag{26}$$

$$\frac{\partial U_3}{\partial t}+\mathbf{v}\cdot\nabla U_3=H_3\left(\left[1-U_{3[0]}^s\right]-U_3\right)^2-I_3U_3^2 \tag{27}$$

$$\frac{\partial U_4^s}{\partial t}+\mathbf{v}\cdot\nabla U_4^s=-I_4^s U_4^s \tag{28}$$

$$\rho\left(\frac{\partial \mathbf{v}}{\partial t}+\mathbf{v}\cdot\nabla\mathbf{v}\right)=\nabla\cdot\boldsymbol{\sigma}+\rho\mathbf{g}. \tag{29}$$

In the above list, the equation of motion is also included to take into account the effects of inertia. Also, in order to calculate the shear rate $\dot{\gamma}$ in correct manner, Eq. (29) has to be solved simultaneously with Eqs. (26)–(28). The term $\boldsymbol{\sigma}=-p\mathbf{I}+2\eta\dot{\boldsymbol{\varepsilon}}$ is the constitutive equation, where the terms p, $\mathbf{I}$, $\mathbf{v}$ and $\dot{\boldsymbol{\varepsilon}}=(\nabla\mathbf{v}+(\nabla\mathbf{v})^T)/2$ are the pressure, the unit dyadic, velocity and the rate-of-deformation tensor, respectively [39,40]. The shear rate is calculated as $\dot{\gamma}=\sqrt{2\dot{\varepsilon}:\dot{\varepsilon}}$ [41–43] (see also [44,45]) and the torque as $T_c=2\pi R_i^2 h\eta\dot{\gamma}$ [16,17]. The terms ρ and $\mathbf{g}$ are the density of the cement paste and gravity, respectively.

Eqs. (26)–(29) are interlinked by the apparent viscosity $\eta=\eta(U_3,U_3^s,U_4^s,\dot{\gamma},\ldots)$ (see Eqs. (16)–(25)), by the rate equations $H_3=H_3(\dot{\gamma},\partial\dot{\gamma}/\partial t)$, $I_3=I_3(\dot{\gamma})$, $I_3^s=I_3^s(\dot{\gamma})$ and $I_4^s=I_4^s(\dot{\gamma})$ (see Eqs. (7)–(9), (11) and (15)), and by the shear rate $\dot{\gamma}=\sqrt{2\dot{\varepsilon}:\dot{\varepsilon}}$. For each computed time step, all these equations have to be (and are) solved simultaneously together. Since U_3^p and U_4^p are constants during a single rheological test, no evolution equations are present for those parameters.

The numerical software used in solving the above set of equations is named Viscometric–ViscoPlastic-Flow 2.0 (see Appendix A.1).

6. Experimental and numerical results

As explained in Section 2, each cement paste is mixed with different type of superplasticizer, i.e. either with VHMW Na, SNF or HMW Na. The purpose of this is to create different rheological response and to test the model equations of the PFI-theory (Section 5) against this response. In this context, the effect of each superplasticizer type is of great relevance. The experimental results T given by the viscometer (solid lines) and the computed results T_c given by the software (double lines) are shown in Figs. 4, 5 and 7. The software VVPF 2.0 (see Appendix A.1) uses the theory presented in Sections 4 and 5, while the viscometer uses the experimental setup presented in Section 2. In the numerical simulations, the values shown in Tables 1, 2 and 3 are used. Four illustrations are presented in Figs. 4, 5 and 7, marked with "t_m=12 min", "t_m=42 min", "t_m=72 min" and "t_m=102 min" (also marked with (a), (b), (c) and (d)) and represent the time from the initial water addition as explained in Section 2.

In the following three sections, the experimental and numerical results for the three different polymer cases VHMW Na, SNF and HMW Na are presented. In addition, the results of the PFI-theory (Mark I) are compared to the outcome of the MHI-theory presented in [16].

6.1. Cement paste mixed with VHMW Na

The solid lines in Fig. 4 represent the measured time-dependent behavior of the cement paste when mixed with the VHMW Na polymer. As explained in [16], each such line is the average result of three repeated batches and is considered to give a good representation of the true material behavior for the cement paste, when mixed with the VHMW Na polymer. The same setup and condition apply for Sections 6.2 and 6.3.

The viscometric values used in the numerical simulation (the double lines) are shown in Table 1. As shown in Fig. 4, there is a good correspondence between the measured torque T and its computed counterpart T_c. This applies for all four illustrations. The computational result presented here is only slightly better than of the MHI-theory presented in [16]. Hence, the benefits of the PFI-theory are not so apparent and will not be so until the cases of SNF and HMW Na are

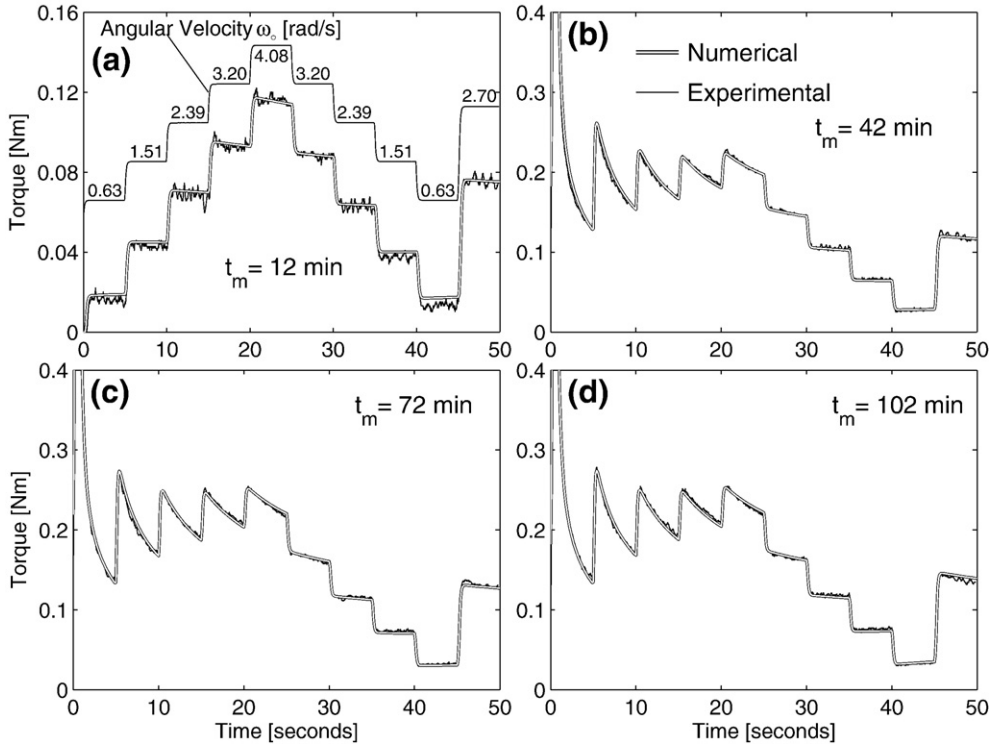

Fig. 4. Measured- and computed torque (VHMW Na-case).

addressed (Sections 6.2 and 6.3). In Table 1 (and in Tables 2 and 3), all values are extracted by the means of "trial and error". That is, all the values are systematically changed by a computer operator until the computed torque can completely overlap the measured torque. For further discussion about this issue, see [16] (Section 4.1).

As shown in Table 1, in reproducing the measured torque in the best fashion, the values of α and β are kept very small for all cases. According to Eqs. (7) and (8), this means that the rate H_3 in which particles collide and stick together (at least for a short while) is very low during a single experiment of 50 s (see Sections 4.1 and 4.4). That

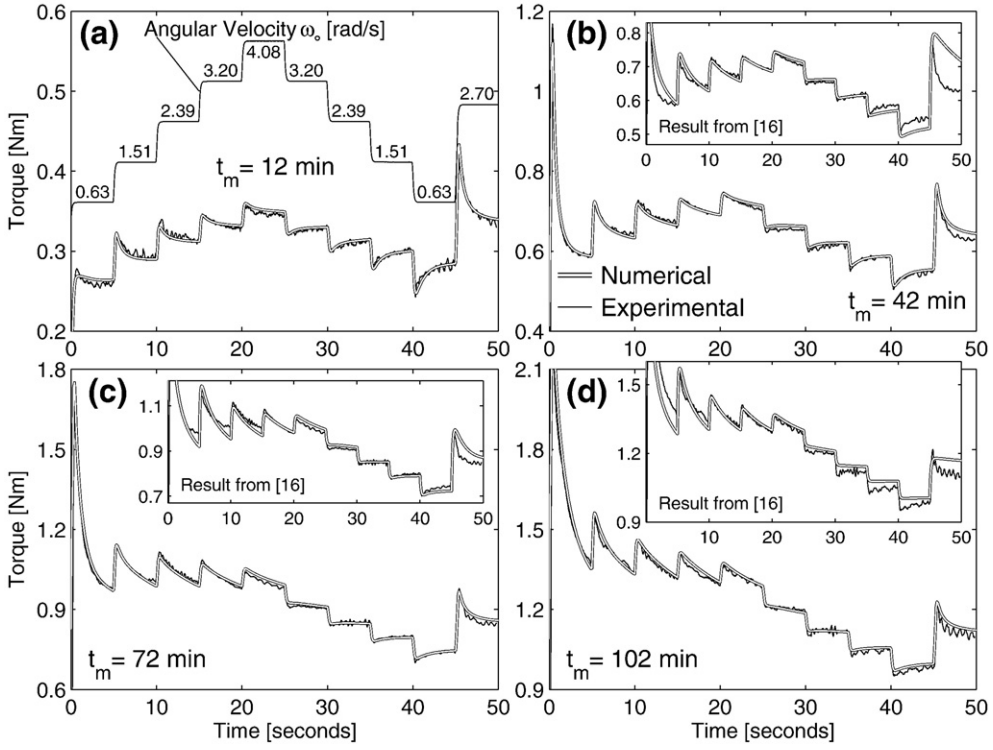

Fig. 5. Measured- and computed torque (SNF-case).

Table 1
Viscometric parameters used in the numerical simulations shown in Fig. 4 (VHMW Na-case)

t_m	μ	τ_0	ξ_I	ξ_{II}	ξ_{III}	ξ_{IV}	ξ_V	ξ_{VI}	α	β	κ	a	λ	χ	$U_{3[0]}$	$U^s_{3[0]}$	$U^s_{4[0]}$
[min]	[Pa·s]	[Pa]	[Pa·s]	[Pa]	[Pa·s]	[Pa]	[Pa·s]	[Pa]	$[s^{-2.99}]$	$[s^{-2.9}]$	$[s^{a-1}]$	[−]	$[s^{-0.6}]$	$[s^{-0.9}]$	[−]	[−]	[−]
Eq.→	(20)	(21)	(22)	(23)	(24)	(25)	(24)	(25)	(8)	(8)	(9)	(9)	(11)	(15)	(13)	(10)	(14)
12	0.28	0.0	18.0	0.0	–	–	–	–	0.001	0.001	0.15	1.0	–	–	0.005	0.00	0.00
42	0.75	0.0	26.0	10.0	4.0	2.0	135.0	40.0	0.001	0.001	0.95	1.0	0.090	3.50	0.900	0.10	1.00
72	0.85	0.0	26.0	10.0	4.0	2.0	175.0	50.0	0.001	0.001	0.95	1.0	0.055	3.50	0.900	0.10	1.00
102	0.85	0.0	26.0	10.0	4.0	2.0	135.0	40.0	0.001	0.006	0.95	1.0	0.055	3.50	0.900	0.10	1.00

Table 2
Viscometric parameters used in the numerical simulations shown in Fig. 5 (SNF-case)

t_m	μ	τ_0	ξ_I	ξ_{II}	ξ_{III}	ξ_{IV}	ξ_V	ξ_{VI}	α	β	κ	a	λ	χ	$U_{3[0]}$	$U^s_{3[0]}$	$U^s_{4[0]}$
[min]	[Pa·s]	[Pa]	[Pa·s]	[Pa]	[Pa·s]	[Pa]	[Pa·s]	[Pa]	$[s^{-2.99}]$	$[s^{-2.9}]$	$[s^{a-1}]$	[−]	$[s^{-0.6}]$	$[s^{-0.9}]$	[−]	[−]	[−]
Eq.→	(20)	(21)	(22)	(23)	(24)	(25)	(24)	(25)	(8)	(8)	(9)	(9)	(11)	(15)	(13)	(10)	(14)
12	0.55	33.5	30+	20+	–	–	–	–	0.000	0.200	0.90	2.3	–	–	0.010	0.00	0.00
42	0.75	78.0	33.0	40.0	1.5	1.0	2.0	0.5	0.400	0.150	0.35	2.3	0.033	1.30	0.800	0.20	1.00
72	0.75	115.0	33.0	40.0	2.5	60.0	6.0	50.0	0.400	0.150	0.35	2.3	0.034	0.95	0.550	0.45	1.00
102	0.75	160.5	33.0	40.0	4.0	70.0	10.0	70.0	0.400	0.150	0.35	2.3	0.033	0.50	0.500	0.50	1.00

is, the contribution from the coagulation rate H_3 is very low when calculating U_3 by Eq. (27). Hence, an increase in the coagulated state U_3 is almost not noticeable in the calculation, which again results in almost no rebuild (or recovery) in the computed torque.

With the very effective dispersing mechanism of the VHMW Na polymer and with the very recent agitation from the initial mixing inside the Hobart mixer (see Section 2), the cement particles are very well dispersed at the start of the rheological experiment at t_m=12 min. Therefore, the initial coagulated state $U_{3[0]}$ is set to $5{\cdot}10^{-3}$ in Table 1. This value is not determined by theoretical means, but rather is determined (in the same manner as all other viscometric values) in the process of reproducing measured torque in the best fashion. The same initial value was used in [16].

In Table 1, it is interesting to note how little evolution there is in the viscometric values as a function of time from water addition. The difference is greatest between the measurement conducted at t_m= 12 min and the rest of the measurements, conducted at t_m=42, 72 and 102 min. The yield stress τ_0 is always equal to zero and the plastic viscosity μ is approximately a constant, equal to about 0.8 Pa·s (excluding the first measurement). In Section 4.6, the plastic viscosity μ and the yield stress τ_0 are considered to be dependent on the permanent coagulated- and linked states U^p_3 and U^p_4. Hence, with τ_0=0 one could suggest that neither the size 3 nor the size 4 cement particles are permanently connected. A similar conclusion was made in [16].

6.2. Cement paste mixed with SNF

The time-dependent behavior of cement paste when mixed with the SNF polymer is shown in Fig. 5 (the black solid line). As always, the computed result is shown with the double line. The viscometric values used in calculating the computed torque are shown in Table 2.

As shown in Fig. 5, a rebuild in torque is measured. In the process of reproducing such behavior by numerical means, the values of α and β are increased by about two orders of magnitude, relative to the VHMW Na-case (see Tables 1 and 2). Although α and β are fitted parameters (see the second paragraph in Section 6.1), they do correspond to a certain physical process. That is, with such an increase in α and β, then by Eqs. (7) and (8), the value of H_3 is roughly increased by two orders of magnitude. This means that the rate in which particles collide and thereafter stick together (at least for a short while) is increased about 100 times (see Sections 4.1 and 4.4). By Eq. (27), such an increase in H_3 results in a significant increase in U_3 during the experiment of 50 s, which again corresponds to the above mentioned rebuild in torque (see Eqs. (22) and (23)).

As shown in Fig. 5, there is a very good correspondence between the measured torque T and its computed counterpart T_c for all the four cases t_m=12, 42, 72 and 102 min. Such (almost) perfect result was not obtained in [16], as is clear when examining the small incorporated illustration in each figure. This clearly demonstrates the improvements of the PFI-theory (Mark I) over the MHI-theory.

For the case of t_m=12 min (Fig. 5a), the measured recovery in torque is extraordinary: When comparing the torque T between 0 and 5 s with the torque between 40 and 45 s, the latter case is higher than the former. Both cases are pointed with arrows in the left illustration of Fig. 6. In either case, the angular velocity ω_o is the same or 0.63 rad/s. Hence, both torque values should approach the same equilibrium line, for example the horizontal line marked with the capital letter A in Fig. 6. That is, the same microstructural equilibrium state should be approached for the same angular velocity ω_o. One way of simulating this extraordinary recovery in torque, is by allowing the coagulated state U_3 to exceed its initial value $U_{3[0]}$. In [16], such approach was considered unphysical and thus never attempted. With the current model, no such restriction is made; i.e. according to Section 4.5.2, the value of U_3 can now reach $1-U^s_3$. More precisely, the physics of the model is now allowed to determine freely the value of U_3 in the range from 0 to $1-U^s_3$. However, regardless of this new approach, then next to

Table 3
Viscometric parameters used in the numerical simulations shown in Fig. 7 (HMW Na-case)

t_m	μ	τ_0	ξ_I	ξ_{II}	ξ_{III}	ξ_{IV}	ξ_V	ξ_{VI}	α	β	κ	a	λ	χ	$U_{3[0]}$	$U^s_{3[0]}$	$U^s_{4[0]}$
[min]	[Pa·s]	[Pa]	[Pa·s]	[Pa]	[Pa·s]	[Pa]	[Pa·s]	[Pa]	$[s^{-2.99}]$	$[s^{-2.9}]$	$[s^{a-1}]$	[−]	$[s^{-0.6}]$	$[s^{-0.9}]$	[−]	[−]	[−]
Eq.→	(20)	(21)	(22)	(23)	(24)	(25)	(24)	(25)	(8)	(8)	(9)	(9)	(11)	(15)	(13)	(10)	(14)
12	0.80	62.0	65.0	25.0	–	–	–	–	0.250	0.200	0.35	2.5	–	–	0.080	0.00	0.00
42	0.53	103.5	50.0	20.0	2.0	1.0	70.0	30.0	0.300	0.600	0.35	2.5	0.050	1.50	0.850	0.15	1.00
72	0.53	123.0	50.0	20.0	4.0	3.0	80.0	60.0	0.300	0.400	0.35	2.5	0.040	1.10	0.850	0.15	1.00
102	0.48	134.0	50.0	20.0	4.0	3.0	75.0	50.0	0.300	0.400	0.35	2.5	0.045	1.30	0.850	0.15	1.00

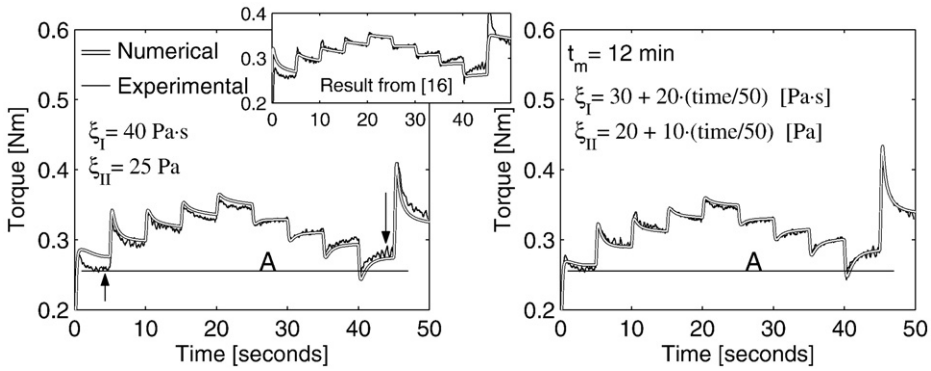

Fig. 6. Two computed results for the SNF-case at t_m = 12 min. To the left, both terms ξ_I and ξ_{II} are kept constant, while to the right, these are set as a function of time t (used in Fig. 5a).

the inner cylinder, where largest shear rate $\dot{\gamma}$ prevails (and torque is calculated), the value of U_3 never exceeds its initial condition of $U_{3[0]}$ = 0.01. Hence, regardless of this new step, the model cannot (without further modification) reproduce the extraordinary recovery in torque. The current attempt is shown in the left illustration of Fig. 6.

Another approach considered in [16] to simulate the large rebuild in measured torque, is by allowing a gradual increase in the two values ξ_I and ξ_{II} (c.f. Eqs. (22) and (23)). As mentioned before, these terms are material parameters depending, among other factors, on the phase volume Φ and surface roughness of the cement particles. The necessity in allowing ξ_I and ξ_{II} to increase could suggest that the apparent phase volume Φ is increasing during the short time interval of 50 s (the surface roughness can safely be considered to be unchanged during the same time interval because of relatively slow cement hydration). The basic idea is that there is a difference between the types of structure for the flocks of cement particles in the beginning between 0 and 5 s, and in the end between 40 and 45 s. An example of such difference is shown with Fig. 8 in [16]. Increasing ξ_I and ξ_{II} as a function of time, gives the result shown in the right illustration of Fig. 6. This approach gives a good match between the measured data and the computed result. This result is also shown in Fig. 5a.

Allowing the material parameters to depend directly on time as done above is unfortunate. The aim has always been to keep them as a constant, or in the worst case, only dependent on other variables used like the shear rate $\dot{\gamma}$ or the coagulated state U_3. It is only here (i.e. for SNF at 12 min) that ξ_I and ξ_{II} are set as non-constants, directly dependent on time t. For this particular case, it was also attempted to let ξ_I and ξ_{II} depend indirectly on time and then through the coagulated state (that is, using $\xi_I = \xi_I(U_3)$ and $\xi_{II} = \xi_{II}(U_3)$). Several such functions were tested without any real success.

6.3. Cement paste mixed with HMW Na

When using the HMW Na polymer in the cement paste, a somewhat larger rebuild in torque is measured relative to the SNF-case. This is apparent when comparing Fig. 7 with Fig. 5. The MHI-

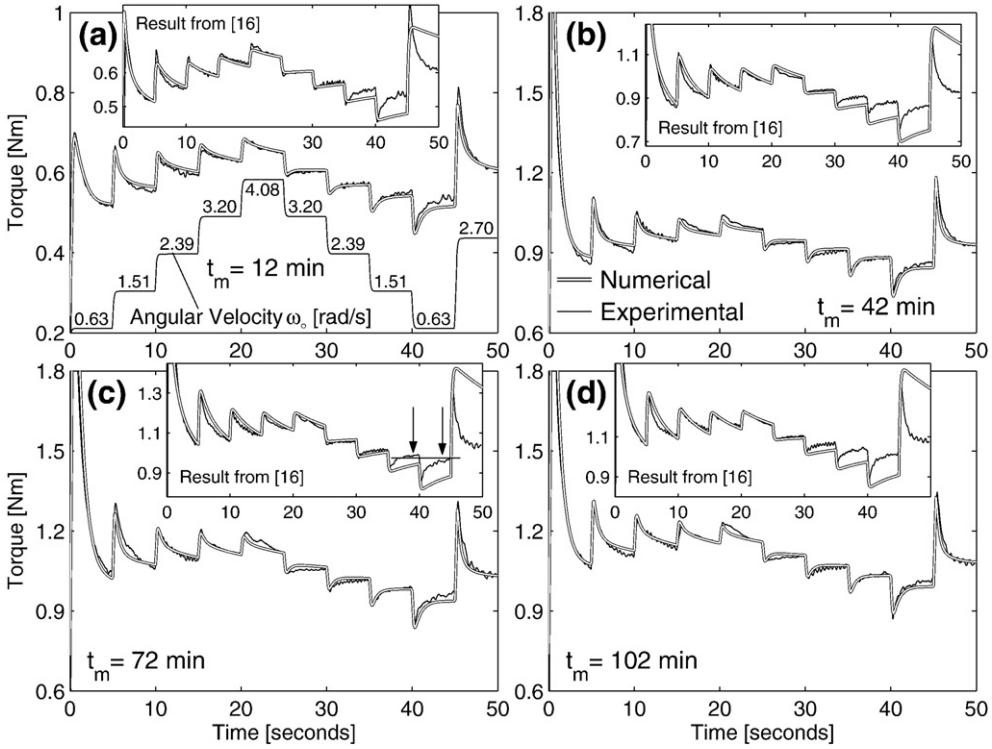

Fig. 7. Measured- and computed torque (HMW Na-case).

theory [16] could not simulate this recovery in torque, while the PFI-theory can. Here, the benefits of the theory are most clear. To calculate the larger recovery, the values of α and β are slightly increased relative to the SNF-case (see Table 3), meaning a somewhat larger coagulation rate H_3 during the calculations.

As is shown with the two arrows in the small incorporated illustration of Fig. 7c, the measured torque T between 40 and 45 s (ω_o=0.63 rad/s) gains almost the same equilibrium value as between 35 and 40 s (ω_o=1.51 rad/s). Such tendency is actually measured for all cases in Fig. 7. This behavior was considered peculiar in [16] because in the former case, the angular velocity ω_o is less than half of the latter case. Nonetheless, as is clear in each of the four main illustrations of Fig. 7, then with the PFI-theory such rebuild in torque is reproduced.

Fig. 8a and b shows the computed shear rate $\dot{\gamma}$ as a function of radius R and time t at 12 and 72 min after water addition, respectively. The white line on the "$\dot{\gamma}$=0"-plane, shows the boundary between the solid state (rigid body motion) and the viscoplastic state (fluid motion). In these two illustrations, the shear rate $\dot{\gamma}$ is at its lowest value near the outer cylinder, while at its highest value next to the inner cylinder (of the viscometer). The combination of low shear rate $\dot{\gamma}$ and large α and β values, gives large coagulation rate H_3 values (see Eqs. (7) and (8)). Through Eq. (27), this means large U_3 values as shown in Fig. 8c and d. For further information about the calculation of shear rate, see Appendix A.2.

Shown in Fig. 8e–h are time evolution of the linked states U_3^s and U_3^s, which are calculated by Eqs. (26) and (28). Comparing Fig. 8f with h, it is clear that U_4^s decreases much faster relative to U_3^s. This indicates that the linkages of the larger cement particles (size 4) are more easily broken relative to the linkages of the smaller cement particles (size 3). In relation to this, it should be clear that the initial values $U_{3[0]}^s$=0.15 and $U_{4[0]}^s$=1 do not necessarily represent a larger number of linkages J between the size 4 cement particles, relative to the size 3 cement particles. The actual number of linkages depends on how many primary particles n are present for each size domain, c.f. $J_3^s=n_3U_3^s$ and $J_4^s=n_4U_4^s$ (see Section 4.3). For example, if $n_3=10^{12}$ m^{-3} and $n_4=10^9$ m^{-3}, then the initial value of J_3^s is $1.5\cdot10^{11}$ m^{-3}, while the initial value of J_4^s is two orders of magnitude less or 10^9 m^{-3}.

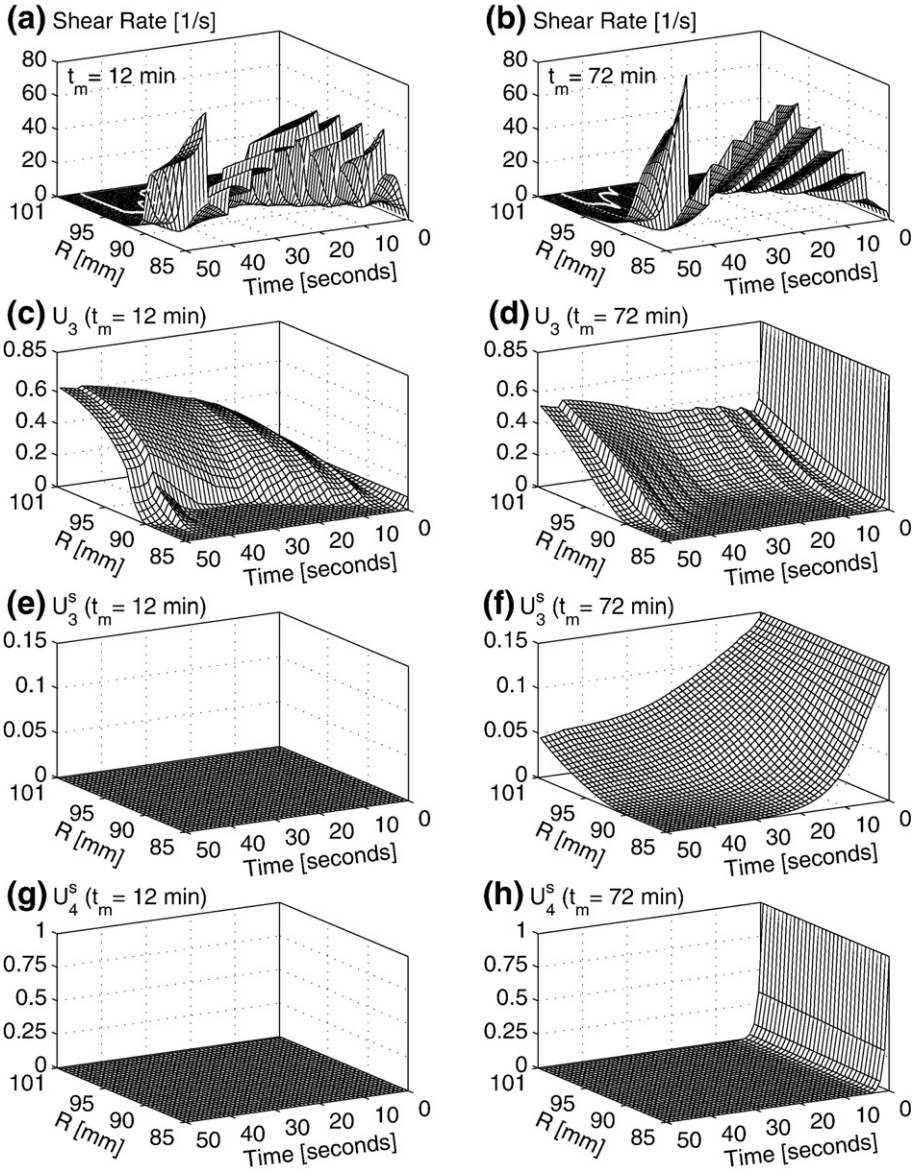

Fig. 8. $\dot{\gamma}$, U_3, U_3^s and U_4^s at t_m=12 min (left) and at 72 min (right); HMW Na-case.

7. Discussions

7.1. Summary of the PFI-theory

In this work a somewhat comprehensive theory (PFI) is presented to simulate the rheological behavior of cement paste. Fig. 9 is a concise visual summary of the main features of this complex theory and should be viewed alongside Fig. 2 and the corresponding text. J_3, J_3^s and J_3^p differ for the three states shown in Fig. 9a–c, which represent cement paste at different stages before setting, and are simplified versions of the paste shown in Fig. 9d. For simplicity, connections between size 4 cement particles are not treated in Fig. 9 and thus neither is J_4^s nor J_4^p (see rather Fig. 2).

Fig. 9a represents the cement paste after some resting (say 10 min, or so). There the connections between the cement particles are of both reversible and permanent nature. Also, some cement particles are still free. With agitation, the cement particles with reversible connections become free, while the cement particles with permanent connections remain connected together. This is shown in Fig. 9b. Allowing the material to rest for another relatively short time period, would allow it to return (more or less) back to the state shown in Fig. 9a. However, with still longer resting time, more and more cement particles would become permanently connected. In the PFI-theory, this last mentioned behavior contributes to the workability loss (see Eqs. (20) and (21) and the adjoining text). In Fig. 9c, most of the cement particles have been permanently connected and thus the cement paste cannot flow, not even with the attempt of re-agitation. For this case, one could say that the material has similar consistency as (somewhat wetted) clay. The cement pastes shown in Fig. 9a and c have a similar consistency. Their difference consists in that the former can be re-agitated to make it flowable, while the latter not. In Fig. 9e, setting has finally occurred with the development of strength. This last mentioned state is outside the scope of the PFI-theory.

7.2. Additional subdivisions of particle sizes

As mentioned in Section 4.3, the system of particles is divided into two particle size domains, designated as size 3 and size 4. It is possible to increase this resolution by further subdividing these two sizes into finer particle domains. Equations for both the coagulated- and linked states of each particle size domain can be based on the results from Section 5. That is, with Eqs. (26)–(28) (including Eq. (12)), the following can be suggested

$$\frac{\partial U_{ij}^s}{\partial t} + \mathbf{v}\cdot\nabla U_{ij}^s = -I_{ij}^s U_{ij}^s \tag{30}$$

$$\frac{\partial U_{ij}}{\partial t} + \mathbf{v}\cdot\nabla U_{ij} = H_{ij}\left(\left[1-U_{ij}^s\right]-U_{ij}\right)^2 - I_{ij}U_{ij}^2 \tag{31}$$

for i and j equal to 1, 2, 3, 4, 5,… N, where each number represents a specific cement particle size domain. As mentioned in Section 4.3, then for historical reason, the numbers “1” and “2” were reserved for water molecules and water adsorption. However, with the above presentation, it is more convenient to ignore this and let i and j equal to 1 represent the smallest cement particle size domain. The maximum value of i and j, namely N, depends on how many particle size domains are defined. The term U_{ij} can be designated with U_i when $i=j$ and represents the coagulated state of cement particles of the same size domain. When $i\neq j$, then U_{ij} represents the coagulated state of cement particles of different size domains. The same applies for the linked state U_{ij}^s.

The problem with the above framework, is that the number of parameters introduced (through H_{ij}, I_{ij} and I_{ij}^s) is rapidly increasing, rendering Eqs. (30) and (31) difficult to use. To complicate the model even further, it is possible to add equations for the permanent

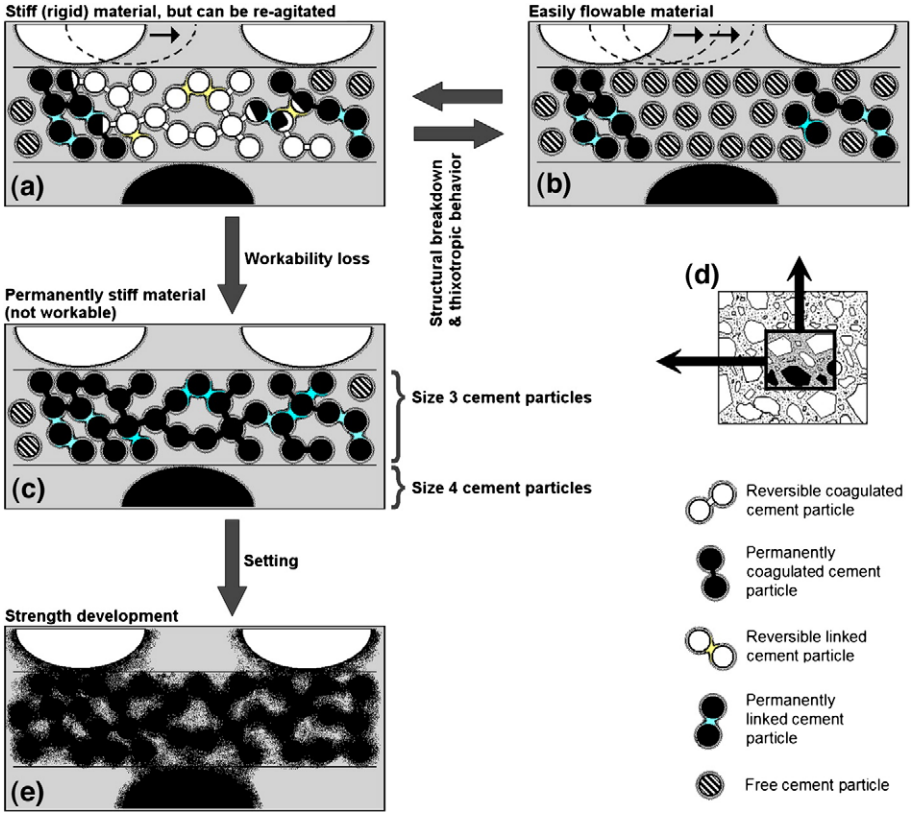

Fig. 9. Visual summary of the most important aspects of the PFI-theory.

coagulated state $U_{ij}^{p,c}$ and for the permanent linked state $U_{ij}^{p,s}$ then with a similar form as the above set of equations (see Section 4.2 about the superscripts "p,c" and "p,s"). This would be done to be able to describe cement based materials behavior when submitted to longer resting times. Although this would give a more complete picture of the overall rheological behavior, the number of parameters would increase still further and make the material model even more difficult to use.

8. Conclusions

A rheological material model is presented to describe time-dependent behavior of the cement paste with different types of admixtures. It is named the *Particle Flow Interaction Theory*, or the PFI-theory. Its current version is designated as "Mark I". The model is an extension of the previous MHI-theory presented in [16] and can better explain transient effects commonly observed in cement pastes. The predictions are compared with experimental data collected during complicated shear flow. A good agreement is observed for all the experiments.

The results highlight the following: Time-dependent behavior of cement paste appears to be mostly governed by combination of coagulation, dispersion and re-coagulation of the cement particles (giving a thixotropic behavior) in combination with breaking of chemically formed linkages between the particles (giving a structural breakdown behavior). This is assumed in the current model, which can successfully reproduce the measured data.

As in [16], it was necessary to introduce different yield stresses into the current model. Three types of yield stresses are introduced, namely τ_0, $\tilde{\tau}_0$ and $\hat{\tau}_0$. The yield stress τ_0 is related to the number of permanent junctions $J_3^{p,c}$ and to chemically formed permanent linkages $J_3^{p,s}$ and J_4^p. Furthermore, the thixotropic yield stress $\tilde{\tau}_0$ is related to the number of reversible junctions J_3, while the yield stress of structural breakdown $\hat{\tau}_0$ is related to chemically formed breakable linkages J_3^s and J_4^s. The same relationship applies for the plastic viscosity variables, μ, $\tilde{\mu}$ and $\hat{\mu}$.

The coagulation rate function H_3 used in the simulation could not be represented with a constant as was done in the original Hattori–Izumi theory [18]. In both theories MHI and PFI, the function $H_3 = K/(\dot{\gamma}^2 + l)$ gives good results. In the MHI-theory, the function K was a step-function that increased and decreased parallel to $d\omega_o/dt$ [16]. However, with the current model, this is no longer the case as K now only depends on intrinsic variables, namely on the shear rate $\dot{\gamma}$ and its time derivative $\partial\dot{\gamma}/\partial t$ (see Eq. (8)).

A physical interpretation of the model results is similar to what was concluded in [16] and may be as follows: Of the three polymer types VHMW Na, SNF and HMW Na, the first one is the most effective in dispersing the cement particles. This is apparent by two facts. First, with zero yield stress τ_0 at all times, the number of permanent junctions and linkages (J_3^p and J_4^p) can be considered to be zero. Secondly, with very small α and β values (see Eqs. (7) and (8)), a very slow rate of coagulation H_3 is occurring during a rheological experiment, meaning that the number of reversible junctions J_3 generally decreases during the 50 s. For the other two cases SNF and HMW Na, the situation is not so simple. With α and β values much larger, the reversible junction number J_3 also increases in some areas (inside the viscometer) during an experiment of 50 s. In addition to this, with non-zero yield stress τ_0, the number of permanent connections (junctions and/or linkages; J_3^p and J_4^p) can be considered larger than for the VHMW Na-case.

In all cases of VHMW Na, SNF and HMW Na, the polymers adsorb on the surface of the cement particles. Their function is to change the total potential energy (see Section 4.1) in such manner that coagulation is more difficultly obtained and dispersion more easily achieved, giving a reduced junction number. Also, with sufficient polymer thickness between the cement particles (i.e. giving enough steric hindrance), the probability for a successful link formation is reduced (see Section 4.7). Hence, with a different type of polymer used, the time evolution of the junction- and link numbers J_3, J_3^s, J_3^p, J_4^s and J_4^p become different, which again results in the different rheological behavior observed.

Acknowledgements

Special thanks to Professor Erik J. Sellevold, who provided the author a postdoctoral research position at the Norwegian University of Science and Technology, NTNU. During that time, the majority of the present work was carried out.

Appendix A. Few computational issues

A.1. The simulation software

The simulation software used in solving Eqs. (26)–(29) is named Viscometric–ViscoPlastic-Flow 2.0, or VVPF 2.0. The source code (which is GNU GPL licensed) is available at www.vvpf.net. It is based on the finite difference method (FDM) and is designed for time-dependent (transient) and time-independent (steady state) viscoplastic materials. In the software, Eqs. (26)–(29) are interlinked by the variables η, H, I_3, I_3^s, I_4^s and $\dot{\gamma}$. Thus, for each computed time step, all these variables, as well as Eqs. (26)–(29), are calculated simultaneously together. That is, each variable is dependent on the outcome of all the others, either directly and/or indirectly (the presence of an indirect dependency is mostly through the equation of motion, Eq. (29)). Such interdependency causes a certain computational problem, which is solved by a method called the successive substitutions, also known as the Picard iteration [42].

Since U_3^p and U_4^p are constants during a single rheological test (of 50 s), no evolution equations are present for those parameters in the software. If the duration of a single rheological test is longer than say 5 min, such evolution equations will however start to become important.

By comparing known analytical results with computed results given by the software VVPF 2.0, its quality is verified for steady state cases only. In verifying accuracy for time dependent cases (where analytical results are generally unknown) the outcome of the new version (VVPF 2.0) has been compared to the outcome of the older version (VVPF 1.0). The accuracy of the latter version has been verified by testing consistency, convergence, numerical convergence and stability [16,17]. In the comparison of VVPF 2.0 and VVPF 1.0, the "total" plastic viscosity $\mu_{[t]}$ and the "total" yield stress $\tau_{0[t]}$ are given by

$$\mu_{[t]} = \mu_0(\theta_1 + \theta_2 \exp[-\theta_3(\dot{\gamma} + \theta_4)t]) \tag{32}$$

$$\tau_{0[t]} = \tau_0(\theta_5 + \theta_6 \exp[-\theta_7(\dot{\gamma} + \theta_8)t]) \tag{33}$$

where the apparent viscosity η is given by Eq. (16). The terms θ_1 to θ_8 are arbitrary constants.

A.2. Calculation of shear rate

As explained in Section 5, the numerical calculation done by VVPF 2.0 consists (among other things) of calculating the flow (i.e. the velocity profile $\mathbf{v}$) inside the viscometer, using Eq. (29). In doing this, it becomes apparent that the velocity $\mathbf{v}$ depends on the material parameters used in the simulation (shown in Tables 1–3). Since the shear rate $\dot{\gamma} = \sqrt{2\dot{\varepsilon} : \dot{\varepsilon}}$ is calculated from the velocity $\mathbf{v}$ (c.f. $\dot{\varepsilon} = (\nabla\mathbf{v} + (\nabla\mathbf{v})^T/2)$), it becomes dependent on the material parameters as well (see [41,42,43]). This is demonstrated in Fig. 8a and b, which shows the computed shear rate $\dot{\gamma}$ as a function of radius R and time t: Although the same angular velocity ω_o is always applied in each rheological test (see Fig. 7a), the shear rate evolution can become quite different from one rheological test to the next. This is because of how the material parameters are changing from one such experiment to the next. For

the MHI-theory, the same type of plot is shown with Fig. 11 in [16], however from a different point of view. Although this last mentioned figure applies for the same case as in Fig. 8a and b, they are nevertheless different. This is simply because of the different material model (and material parameters) used and hence different computed response attained.

The white line on the "$\dot{\gamma}$=0"-plane, shown in Fig. 8a and b, demonstrates the boundary between the solid state (rigid body motion) and the viscoplastic state (fluid motion). It is located by plotting the function $-II_s = C_y$ where II_s is the second deviator stress invariant and C_y is the yield condition equal to $\tau_{0[t]}^2$ in this study (see the von Mises yield theory [40]). Such a boundary will make an additional influence on the shear rate $\dot{\gamma}$. This is because of how the thickness of the flow is dynamically increasing and decreasing; i.e. the effective outer radius of the viscometer is changing (with a maximum value of R_o=101 mm).

References

[1] G.H. Tattersall, P.F.G. Banfill, The Rheology of Fresh Concrete, Pitman Books Limited, Great Britain, 1983.
[2] P. Billberg, Form pressure generated by self-compacting concrete — influence of thixotropy and structural behaviour at rest, Ph.D. thesis, Department of Structural Engineering, The Royal Institute of Technology, Stockholm, 2006.
[3] J. Mewis, Thixotropy — a general review, J. Non-Newtonian Fluid Mech. 6 (1979) 1–20.
[4] H.A. Barnes, J.F. Hutton, K. Walters, An Introduction to Rheology, Elsevier Science, Amsterdam, 1989.
[5] H.A. Barnes, Thixotropy — a review, J. Non-Newtonian Fluid Mech. 70 (1997) 1–33.
[6] A. Mujumdar, A.N. Beris, A.B. Metzner, Transient phenomena in thixotropic systems, J. Non-Newtonian Fluid Mech. 102 (2002) 157–178.
[7] R.I. Tanner, K. Walters, Rheology: An Historical Perspective, Elsevier Science, Amsterdam, 1998.
[8] P.F.G. Banfill, The rheology of fresh mortar, Mag. Concr. Res. 43 (154) (1991) 13–21.
[9] K.H. Khayat, J. Assaad, Use of rheological properties of SCC to predict formwork pressure, in: S.P. Shah (Ed.), Proceedings of the Second North American Conference on the Design and Use of Self-Consolidating Concrete (SCC) and the Fourth International RILEM Symposium on Self-Compacting Concrete, Chicago, 2005, pp. 671–677.
[10] R. Lapasin, A. Papo, S. Rajgelj, The phenomenological description of the thixotropic behavior of fresh cement pastes, Rheol. Acta 22 (1983) 410–416.
[11] D.H. Cheng, F. Evans, Phenomenological characterization of the rheological behaviour of inelastic reversible thixotropic and antithixotropic fluids, Br. J. Appl. Phys. 16 (1965) 1599–1617.
[12] P. Coussot, Q.D. Nguyen, H.T. Huynh, D. Bonn, Avalanche behavior in yield stress fluids, Phys. Rev. Lett. 88 (2002) 175501 (4 pages).
[13] N. Roussel, Steady and transient flow behaviour of fresh cement pastes, Cem. Concr. Res. 35 (2005) 1656–1664.
[14] N. Roussel, A thixotropy model for fresh fluid concretes: theory, validation and applications, Cem. Concr. Res. 36 (2006) 1797–1806.
[15] G.H. Tattersall, The rheology of Portland cement pastes, Br. J. Appl. Phys. 6 (1955) 165–167.
[16] J.E. Wallevik, Thixotropic investigation on cement paste: experimental and numerical approach, J. Non-Newtonian Fluid Mech. 132 (2005) 86–99.
[17] J.E. Wallevik, Rheology of particle suspensions — fresh concrete, mortar and cement paste with various types of lignosulfonates, Ph.D. thesis, Department of Structural Engineering, The Norwegian University of Science and Technology, Trondheim, 2003, www.diva-portal.org.
[18] K. Hattori, K. Izumi, Rheology of fresh cement and concrete, in: P.F.G. Banfill (Ed.), Rheology of Fresh Cement and Concrete, Proc. of the International Conference Organized by The British Society of Rheology, University of Liverpool, 16–29 March 1990, E & FN Spon, London, 1991, pp. 83–92.
[19] K. Hattori, K. Izumi, A rheological expression of coagulation rate theory, parts 1–3, J. Dispersion Sci. Technol. 3 (2) (1982) 129–193.
[20] O.H. Wallevik, O.E. Gjørv, Development of a coaxial cylinder viscometer for fresh concrete, properties of fresh concrete, Proceedings of the RILEM Colloquium, University Press, Cambridge, Great Britain, 1990, pp. 213–224.
[21] P.F.G. Banfill, D. Beaupré, F. Chapdelaine, F. de Larrard, P. Domone, L. Nachbaur, T. Sedran, O.H. Wallevik, J.E. Wallevik, Comparison of concrete rheometers: international tests at LCPC (Nantes, France) in October, 2000 (NISTIR 6819), in: F. Ferraris, L.E. Brower (Eds.), National Institute of Standard and Technology (NIST), Gaithersburg, USA, 2001.
[22] A.W. Saak, H.M. Jennings, S.P. Shah, The influence of wall slip on yield stress and viscoelastic measurements of cement paste, Cem. Concr. Res. 31 (2001) 205–212.
[23] N.Q. Dzuy, D.V. Boger, Yield stress measurement for concentrated suspensions, J. Rheol. 27 (4) (1983) 321–349.
[24] J. Yan, A.E. James, The yield surface of viscoelastic and plastic fluids in a vane viscometer, J. Non-Newtonian Fluid Mech. 70 (1997) 237–253.
[25] M. Keentok, J.F. Milthorpe, E. O'Donovan, On the shearing zone around rotating vanes in plastic liquids: theory and experiment, J. Non-Newtonian Fluid Mech. 17 (1985) 23–35.
[26] H.A. Barnes, Q.D. Nguyen, Rotating vane rheometry — a review, J. Non-Newtonian Fluid Mech. 98 (2001) 1–14.
[27] J.E. Wallevik, Microstructure-rheology: thixotropy and workability loss, Nordic Concr. Res. 31 (2004) 16–29.
[28] R.J. Hunter, Foundations of Colloid Science, 2nd edition, Oxford University Press, New York, 2001.
[29] P.F.G. Banfill, D.C. Saunders, On the viscometric examination of cement pastes, Cem. Concr. Res. 11 (3) (1981) 363–370.
[30] P.F.G. Banfill, The rheology of fresh cement and concrete — a review, in: G. Grieve, G. Owens (Eds.), Proc. of the 11th International Congress on the Chemistry of Cement: Cement's Contribution to the Development in the 21st Century, Durban, 11–16 May 2003, 2003.
[31] H.F.W. Taylor, Cement Chemistry, 2nd edition, Thomas Telford Publishing, Great Britain, 1997.
[32] D.J. Shaw, Introduction to Colloid & Surface Chemistry, 4th edition, Reed Educational and Professional Publishing Limited, Great Britain, 1992.
[33] R.A. Bagnold, Experiments on a gravity-free dispersion of large solid spheres in a Newtonian fluid under shear, Proc. Roy. Soc. Lond. A 225 (1954) 49–63.
[34] E.J.W. Verwey, J.Th.G. Overbeek, Theory of the Stability of Lyophobic Colloids, Elsevier Publishing Co. Ltd., Amsterdam, 1948.
[35] J.E. Wallevik, Minimizing end-effects in the coaxial cylinders viscometer: viscoplastic flow inside the ConTec BML Viscometer 3, J. Non-Newtonian Fluid Mech. (in press), doi:10.1016/j.jnnfm.2008.05.006.
[36] M. Bercovier, M. Engelman, A finite element method for incompressible non-Newtonian flows, J. Comput. Phys. 36 (1980) 313–326.
[37] A.J. Taylor, S.D.R. Wilson, Conduit flow of an incompressible, yield-stress fluid, J. Rheol. 41 (1) (1997) 93–101.
[38] G.R. Burgos, A.N. Alexandrou, V. Entov, On the determination of yield surfaces in Herschel–Bulkley fluids, J. Rheol. 43 (3) (1999) 463–483.
[39] L.E. Malvern, Introduction to the Mechanics of Continuous Medium, Prentice-Hall Inc., New Jersey, 1969.
[40] G.E. Mase, Schaums Outline Series: Theory and Problems of Continuum Mechanics, McGraw-Hill Inc., New York, 1970.
[41] C.R. Beverly, R.I. Tanner, Numerical analysis of three-dimensional Bingham plastic flow, J. Non-Newtonian Fluid Mech. 42 (1992) 85–115.
[42] H.P. Langtangen, Computational Partial Differential Equations, Numerical Methods and Diffpack Programming, Lecture Notes in Computational Science and Engineering, Springer-Verlag, Berlin, 1999.
[43] F. Irgens, Continuum Mechanics, Springer-Verlag, Berlin, 2008.
[44] J.G. Oldroyd, A rational formulation of the equations of plastic flow for a Bingham solid, Proc. Camb. Philos. Soc. 43 (1947) 100–105.
[45] J.G. Oldroyd, Two-dimensional plastic flow of a Bingham solid, Proc. Camb. Philos. Soc. 43 (1947) 383–395.